MOFs-drived yolk-shell Ni/C architectures assembled by Ni@C core-shell nanoparticles for lightweight microwave absorbents

Xiaolei Wang,[a*] Qiyao Geng,[a] Guimei Shi,[a] Yajing Zhang[b] and Da Li[*c]

[a]School of Environmental and Chemical Engineering, Shenyang University of Technology, Shenyang 110870, PR China.

[b]College of Chemical Engineering, Shenyang University of Chemical Technology, Shenyang 110142, PR China.

[c]Shenyang National Laboratory for Materials Science, Institute of Metal Research, and International Centre for Materials Physics, Chinese Academy of Sciences, Shenyang 110016, PR hina.

[*] Corresponding author:

E-mail: xlwang@alum.imr.ac.cn; dali@imr.ac.cn

Fax:(+86) 24-25496502 Tel: (+86) 24-25496502

Figure captions

Figure S1 SEM images of Ni-MOF with different ratio of nickle and trimesic acid. (a)1.5:0.5 and (b)1.5:2.

Figure S2 SEM images of Ni-MOF with different amount of PVP. (a) 1.2 g, (b) 2.0 g and (c) 2.5 g.

Figure S3 XRD patterns of Ni-MOF with different reaction time. (a) 2 h, (b) 5 h and (c) 8 h.

Figure S4 TEM images of Ni-MOF with prolonged reaction time: (a) 18 h and (b) 24 h

Figure S5 SEM and TEM images: (a) and (b) NC1, (c) and (d) NC3.

Figure S6 Raman spectroscopy of Ni/C composites. (a)NC1; (b)NC2; (c) NC3.

Figure S7 (a-c) N_2 absorption-desorption isotherms of the Ni/C composites and (d-f) their pore-size distribution.

Figure S8 (a) XRD pattern and (b) SEM image of the etched NC2.

Figure S9 Comparison of electromagnetic parameters of NC2 and the etched NC2.

Figure S10 The etched NC2:(a) impedance matching, (b) attenuation coefficient and (c) microwave absorption.

Table captions

Table S1 Comparison of microwave absorption properties of yolk-shell Ni/C microspheres with other microwave absorbers.

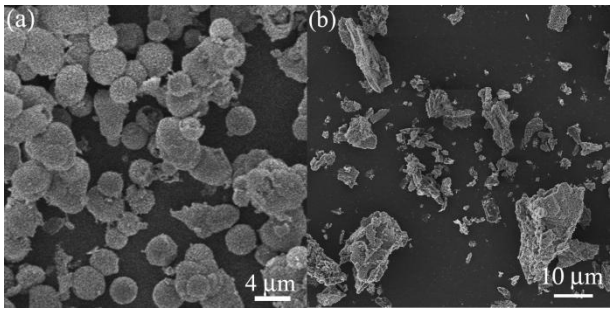

Figure S1 SEM images of Ni-MOF with different ratio of nickle and trimesic acid. (a)1.5:0.5 and (b)1.5:2.

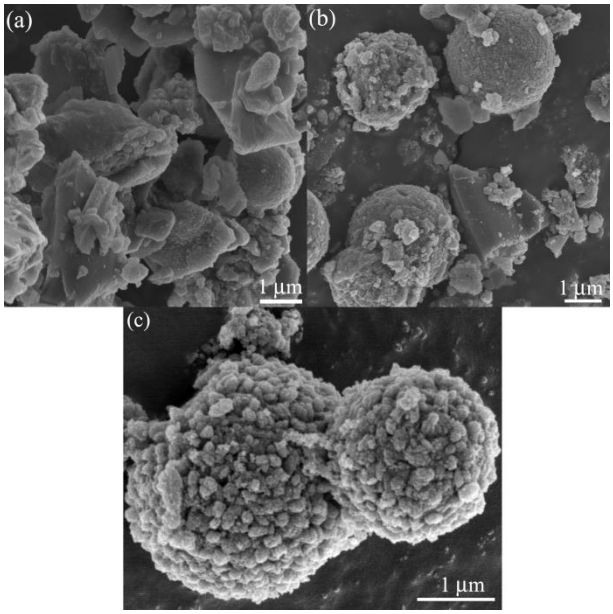

Figure S2 SEM images of Ni-MOF with different amount of PVP. (a) 1.2 g, (b) 2.0 g and (c) 2.5 g.

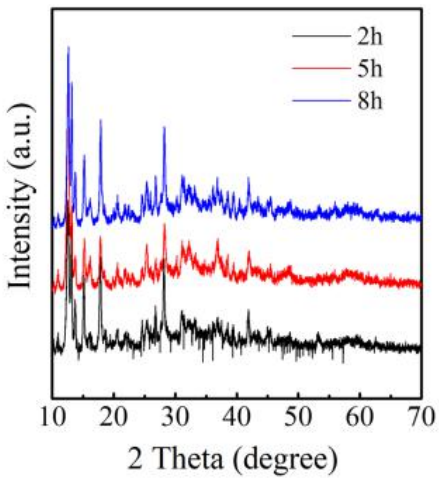

Figure S3 XRD patterns of Ni-MOF with different reaction time. (a) 2 h, (b) 5 h and (c) 8 h.

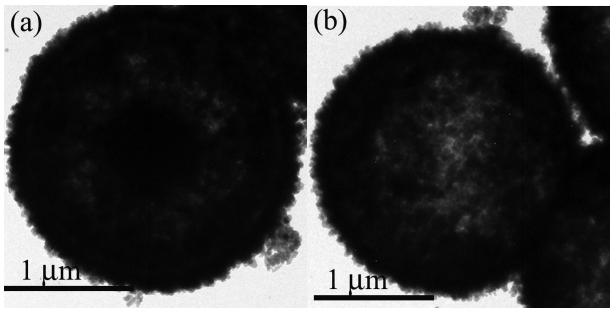

Figure S4 TEM images of Ni-MOF with prolonged reaction time: (a) 18 h and (b) 24 h

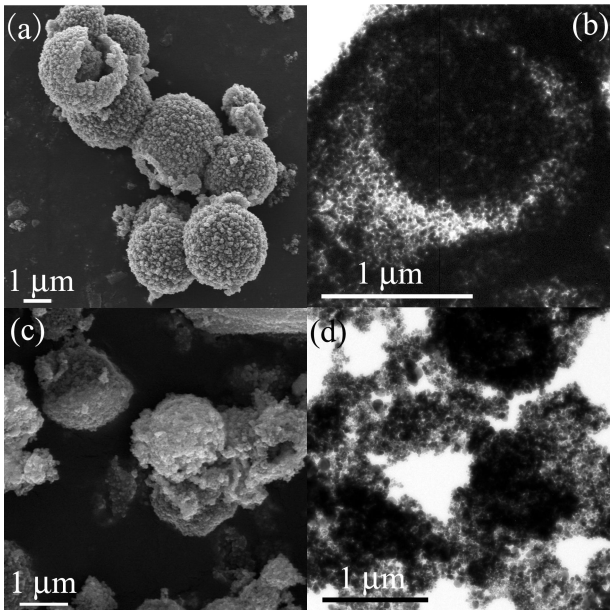

Figure S4 SEM and TEM images: (a) and (b) NC1, (c) and (d) NC3.

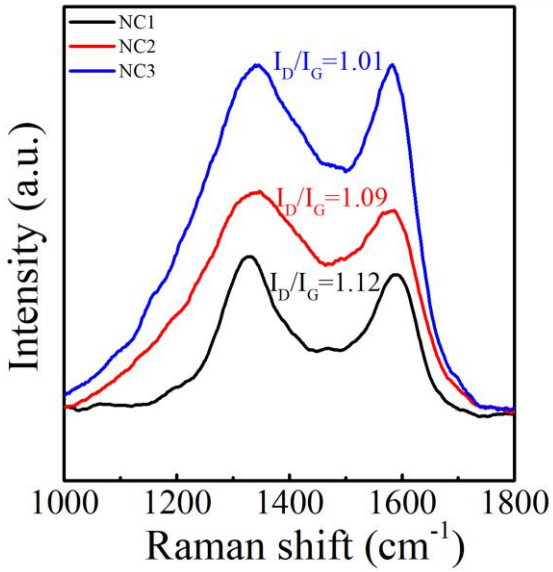

Figure S5 Raman spectroscopy of Ni/C composites. (a)NC1; (b)NC2; (c) NC3.

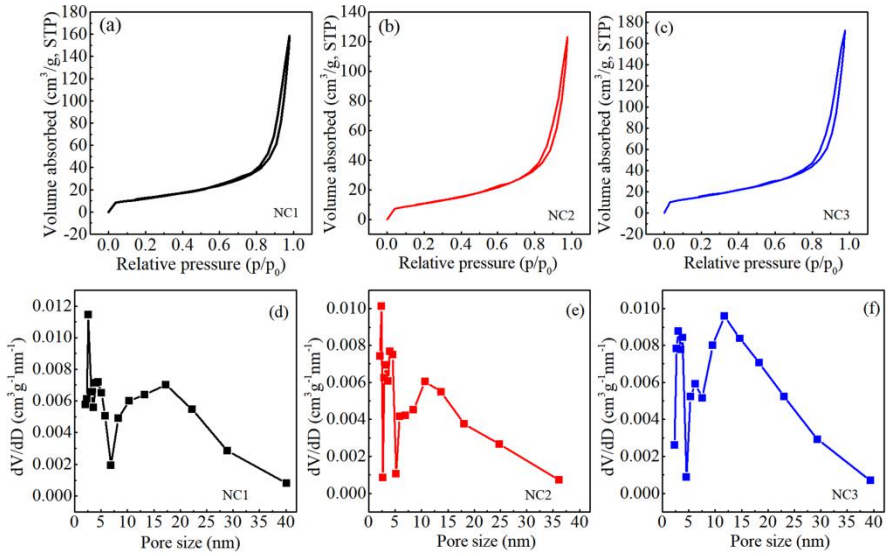

Figure S6 (a-c) N_2 absorption-desorption isotherms of the Ni/C composites and (d-f) their pore-size distribution.

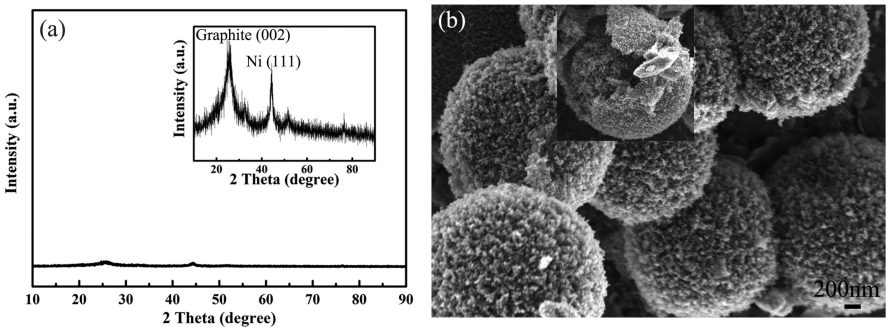

Figure S7 (a) XRD pattern and (b) SEM image of the etched NC2.

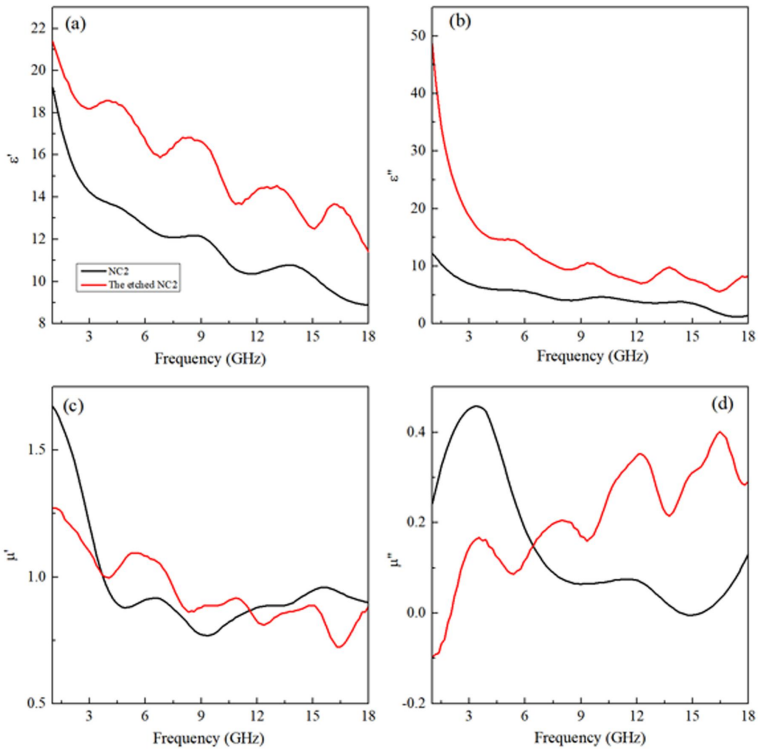

Figure S8 Comparison of electromagnetic parameters of the NC2 and the etched NC2.

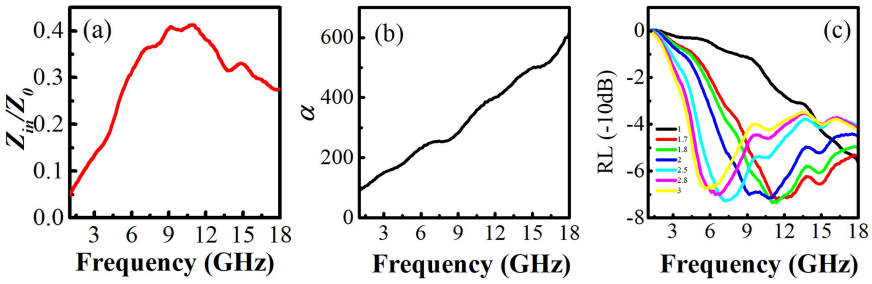

Figure S9 The etched NC2: (a) impedance matching, (b) attenuation coefficient and (c) microwave absorption.

Table S1 Comparison of microwave absorption properties of yolk-shell Ni/C microspheres with other microwave absorbents.

Absorbers	Absorber thickness (mm)	RL (dB)	Frequency (GHz)	Bandwidth (RL< -10 dB) and integrated thickness (mm)	Ref.
Yolk-shell Co_3Fe_7@C	2.0	-35.3	9.1	6.3, 1.5-3.0	1
Yolk-shell C@C	2.0	-34.8	15.0	5.4, 1.0-5.0	2
Porous CF/Carbon Nanofibers	2.3	-31.0	9.7	3.0, 2.3-3.0	3
Co/NPC@void@CI	2.2	-49.2	13.7	11.3, 1.8-2.8	4
MOFs-drieved Co/ZnO/C microrods	3.0	-52.6	4.9	12.5, 1.5-5.0	5
Fe_3O_4@polypyrrole	2.5	-31.5	15.5	5.2, 3.0-5.0	6
Ni@SnO_2	1.8	-45.0	13.9	3.8, 1.5-3.5	7
$ZnFe_2O_4$@SiO_2@RGO	2.8	-43.9	13.9	12.0, 2.0-5.0	8
Fe@ZnO	2.65	-21.5	15.2	9.8, 2.30-4.56	9
Fe/Fe_3O_4@C	2.0	-32.9	17.1	12.8, 2.0-5.0	10
CoFe@C/RGO	3.0	-36.1	13.0	~11.0, 1.7-5.0	11
NC2	1.8	-39.0	13.1	12.3, 1.4-3.9	This work

References

1. H. Li, S. Bao, Y. Li, Y. Huang, J. Chen, H. Zhao, Z. Jiang, Qi. Kuang, Z. Xie, Optimizing the electromagnetic wave absorption performances of designed CoFe@C yolk-shell Structures, ACS Appl. Mater. Interfaces 10 (2018) 28839-28849.
2. R. Qiang, Y. Du, Y. Wang, N. Wang, C. Tian, J. Ma, P. Xu, X. Han, Rational design of yolk-shell C@C microspheres for the effective enhancement in microwave absorption, Carbon 98 (2016) 599-606.
3. G. Ji, T. Xie, S. Yang, J. Jin, J. Jiang, Microwave absorption enhancement of porous carbon fibers compared with carbon nanofibers, J. Phys. Chem. 116 (2012) 9196-9201.
4. B. Quan, X. Liang, G. Ji, J. Ma, P. Ouyang, H. Gong, G. Xu, Y. Du, Strong electromagnetic wave response derived from the construction of dielectric/magnetic media heterostructure and multiple interfaces, ACS Appl. Mater. Interfaces 9 (2017) 9964-9974.
5. Q. Liao, M. He, Y. Zhou, S. Nie, Y. Wang, S. Hu, H. Yang, H. Li, Y. Tong, Highly cuboid-shape heterobimetallic metal-organic frameworks derived from porous Co/ZnO/C microrods with improved electromagnetic wave absorption capabilities, ACS Appl. Mater. Interfaces 10 (2018) 29136-29144.
6. M. Qiao, X. Lei, Y. Ma, L. Tian, K. Su, Q. Zhang, Well-defined core-shell Fe_3O_4@polypyrrole composite microspheres with tunable shell thickness: synthesis and their superior microwave absorption performance in the Ku band, Ind. Eng. Chem. Res. 55 (2016) 6263-6275.
7. B. Zhao, B. Fan, G. Shao, W. Zhao, R. Zhang, Facile synthesis of novel heterostructure based on SnO_2 nanorods grown on submicron Ni walnut with tunable electromagnetic wave absorption capabilities, ACS Appl. Mater. Interfaces 7 (2015) 18815-18823.
8. J. Feng, Y. Hou, Y. Wang, L. Li, Synthesis of hierarchical $ZnFe_2O_4$@SiO_2@RGO core-shell microspheres for enhance electromagnetic wave absorption, ACS Appl. Mater. Interfaces 9 (2017) 14103-14111.
9. J. Wang, Z. Wang, R. Liu, Y. Li, X. Zhao, X. Zhang, Heterogeneous interfacial polarization in Fe@ZnO nanocomposites induces high-frequency microwave absorption, Mater. Lett. 209 (2017) 276-279.
10. X. Jian, X. Xiao, L. Deng, W. Tian, X. Wang, N. Mahmood, S. Dou, Heterostructured nanorings of Fe-Fe_3O_4@C hybrid with enhanced microwave absorption performance, ACS Appl. Mater. Interfaces 10 (2018) 9369-9378.
11. S. Li, Y. Huang, D. Ling, N. Zhang, M. Zong, X. Qin, P. Liu, Enhanced microwave-absorption with carbon-encapsulated Fe-Co particles on reduced graphene oxide nanosheets with nanoscale-holes in the basal plane, J. Colloid Interf. Sci. 544 (2019) 188-197.